Research on Chemical Intermediates (2021) 47:1239–1251
https://doi.org/10.1007/s11164-020-04352-z

The effects of dopant on catalytic activity of Pd/mesoporous alumina for toluene oxidation

Chengyan Ge[1,2] · Lixia Xu[2] · Jingfang Sun[2] · Hongxia Liu[1] · Qing Tong[2] · Weixin Zou[2] · Changjin Tang[2] · Haiqin Wan[2] · Lin Dong[2] · Yu-Wen Chen[3]

Received: 3 August 2020 / Accepted: 3 December 2020 / Published online: 3 January 2021

Abstract

A series of mesoporous alumina (MA) doped with acidic (Ti, W) or alkaline earth (Ba, Mg) elements were prepared. They were used as the supports for Pd catalysts. These catalysts were characterized by N_2 sorption, X-ray diffraction, transmission electron microscopy, X-ray photoelectron spectroscopy, infrared spectroscopy of CO adsorption and temperature-programmed reduction. Complete oxidation of toluene on these catalysts was tested in a fixed-bed micro-reactor. The results of in situ IR of CO adsorption indicated that the doping of basic element was beneficial for the dispersion of PdO particles, while the doping of acid element suppressed the dispersion of PdO particles. The binding energy of Pd in Pd/Ba-MA shifted to high energy, indicating that the interaction between PdO and support was enhanced. The results of H_2-TPR showed that the reducibility of PdO doped with alkaline element was stronger than those of catalysts doped with acidic element. The doping of basic elements promoted the dispersion of PdO particles, changed the electronic state of Pd and enhanced the reducibility of PdO, which led to its high activity. The catalysts doped with the basic elements had higher activities than those doped with acidic elements, among which the Pd/Ba-MA catalyst had the highest activity among all catalysts.

Keywords Mesoporous alumina · Effect of support · Catalytic activity · Toluene oxidation · Pd catalyst

✉ Haiqin Wan
wanhq@nju.edu.cn

✉ Yu-Wen Chen
ywchen@cc.ncu.edu.tw

Extended author information available on the last page of the article

Introduction

Toluene is widely used in the chemical industry [1, 2]. It is a typical volatile organic compounds (VOCs) pollutant, which is not only harmful to human health, but also causes environmental pollution [3, 4]. Catalytic oxidation of toluene was an effective method for toluene elimination [5–7]. Many catalysts have been used for the oxidation of toluene [8–12]. Among them, noble-metal-based catalysts are considered as the best ones for the oxidation of toluene. However, it is too expensive to widely application due to its scarcity of noble metal. Thus, modifying the catalyst supports and reducing the loading amount of noble metal are an effective way to solve the problem [13].

Pd is widely used as an active component in industrial catalysts for the removal of VOCs [14]. Numerous studies have shown that the particle size of Pd, valence state of Pd, Pd loading, oxygen vacancy of the carrier, the acid base of the carrier surface, specific surface area of the carrier, preparation method and pretreatment method of the catalyst all have effects on the performance of the catalyst [15–18]. Huang et al. [19] prepared a series of γ-Al_2O_3 supported precious metals (Pd, Pt, Au, Ag, Rh) catalysts by impregnation method and applied them to the catalytic oxidation of o-xylene, among which Pd/Al_2O_3 had the highest activity. Alvarez et al. [20, 21] prepared Al_2O_3-supported Mn, Pd-Mn and Pd–Ni oxide catalysts for combustion of formaldehyde/methanol mixtures and natural gas to C_2 product. The complete combustion temperature of formaldehyde/methanol mixture on Pd/Al_2O_3 catalyst was 220 °C, while the complete combustion temperature of bimetallic 0.1% Pd-Mn/Al_2O_3 catalyst decreased sharply to 90 °C, and that of 0.4% Pd-Mn/Al_2O_3 catalyst decreased to 80 °C. The better performance of Pd-based catalysts was attributed to the fact that PdO provided not only oxygen but also some metal sites for VOCs decomposition. Many scholars have introduced additives into Pd-based catalysis in order to improve the activity of Pd-based catalysts. The catalyst supports can affect the catalytic activity of noble-metal catalysts. The main role of support is to help the dispersion of metal, and to interact with metal nanoparticles to influence the catalytic activity. The porous support has regular pore structure, narrow pore size distribution and large specific surface area, which is conducive to the dispersion of metal [22, 23]. Ilieva et al. [24] reported that the mesoporous structure of the titania support played an important role in reducing the size of gold particles, making its better catalytic performance for benzene oxidation. Mesoporous alumina (MA) is a relatively new class of carrier materials with high specific surface area, characterized by narrow distribution of mesoporous size, and in selected cases, having nanoscale ordered pore structure [25, 26]. In general, due to the stabilization of active Pd substances on the porous structure and the formation of dispersed Pd metal particles, the porous carrier increases the activity of Pd-based catalysts [27, 28]. Due to its higher specific surface area, the density of active sites in MA is also higher.

One of the key parameters for the development of catalysts is the property of the carrier, which plays an important role in improving the activity and durability of the supported noble metals and is of great significance for surface properties

and metal–carrier interactions. The activity of Pd-based catalysts is generally increased due to the stabilization of active Pd substances on porous structures [29, 30]. The acid–base properties of the carrier can affect the activity of Pd-based catalyst, while the weak acid carrier can improve the catalytic activity [28]. Except for the Bronsted acid and Lewis acid sites, these materials have relatively high density of basic sites compared with conventional alumina. The basic site enhances the strong interaction between the metal oxide (used for oxidation and partial oxidation reactions) and the alumina carrier, thus enhancing the catalytic activity of the catalyst. Due to its high surface area, MA can support higher metal, metal oxide and metal sulfide loads while maintaining a high dispersion of the active phases.

Doping of carrier can enhance the interaction between Pd and the carrier and promote the dispersion of Pd on the surface of the carrier [31]. Zhang et al. [32] studied the catalytic activity of Na-doped Pd/TiO_2 catalyst for HCHO oxidation and reported that Na doping significantly promoted the catalytic activity of Pd/TiO_2 catalyst. At 25 °C, the conversion rate of HCHO was close to 100% on the Na-Pd/TiO_2 catalyst. The results showed that the addition of Na substances could induce the formation and stability of negative charge and well-dispersed Pd substances, which was beneficial to the activation of surface hydroxyl groups and chemisorption oxygen.

In this work, MA doped with various acid (Ti, W) and alkaline earth (Ba, Mg) elements were synthesized. Pd catalysts supported on dopant-modified MA were prepared. The effects of dopant of support on the activity of Pd catalysts were investigated. The catalysts were characterized by BET, TEM, XRD, XPS, in situ CO-IR and H_2-TPR. Toluene oxidation was used to test their catalytic activities.

Experimental

Catalyst preparation

Synthesis of mesoporous alumina (MA) and X-MA(X = Mg, Ti, Ba and W)

At room temperature, 4.0 g P123 was dissolved in 80 ml of ethanol, and Pluronic P123 is a symmetric triblock copolymer comprising poly(ethylene oxide) (PEO) and poly(propylene oxide) (PPO) in an alternating linear fashion, PEO-PPO-PEO. 6.4 ml HNO_3 and 36 mmol of isopropanol aluminum were added in the above solution. The mixed solution was stirred for 5 h, then filtered and dried at 60 °C for 48 h. The final gel was ground to powder and then calcined at 700 °C for 4 h in a muffle furnace with a heating ramp of 2 °C/min to obtain mesoporous alumina (MA).

For the synthesis of X-MA (X = Mg, Ti, Ba, W), the process is the same as that of MA, except adding certain amount of metal salt solution to the mixed solution. Here, $Mg(NO_3)_2$, $Ti(OC_4H_9)_4$, $Ba(NO_3)_2$ and Na_2WO_4 were used as the precursors of X, respectively, and the loading of M was 5.0 wt%.

Synthesis of Pd/X-MA (X = Mg, Ti, Ba and W)

Supported Pd catalyst was prepared by incipient-wetness impregnation method. Suitable amount of $PdCl_2$ solution was added to the X-MA powder with stirring, and it was dried in a water bath at 80 °C. After drying in an oven at 110 °C for 12 h, the catalyst was ground and calcined at 400 °C for 4 h in a muffle furnace. The obtained catalyst was denoted as Pd/X-MA (X = Mg, Ti, Ba, W), and the loading of Pd was 1.0 wt%.

Catalyst characterization

The catalysts were characterized by X-ray diffraction on a Philips Xpert Pro diffraction meter (PANalytical, Netherlands) using Cu K_α radiation ($\lambda = 1.5408$ Å) at 40 kV and 40 mA. The 2θ scan range was from 10° to 80° with the scan rate of 5° min^{-1}. The specific surface area and pore size distribution of the samples were measured by N_2 adsorption–desorption at 77 K on an ASAP 2020 instrument (Micromeritics Instrument Co., Norcross, USA) and calculated by the Brunauer–Emmett–Teller (BET) and Barrett–Joyner–Halenda (BJH) methods. Transmission electron microscope (TEM) experiments were carried out on a JEM-200CX instrument operating at 200 kV. The binding energies of the samples were determined by X-ray photoelectron spectroscopy on an ESCALAB250Xi (Thermo Scientific, USA) with a monochromatized Al K_α excitation source ($h\nu = 1486.6$ eV). The electron binding energy was calibrated by the C_{1s} peak at 284.6 eV. Hydrogen temperature-programmed reduction (H_2–TPR) experiment was performed on a Finesorb-3010 instrument (Fantai, China), equipped with a thermal conductivity detector (TCD). During experiment, 100 mg sample was loaded into a quartz tube and preheated at 110 °C in a N_2 flow (50 ml min^{-1}) for 1 h. Subsequently, the sample was cooled to the room temperature, 10% H_2/Ar mixed gas (50 ml min^{-1}) was switched to the sample cell, and the sample was heated to 200 °C at a rate of 10 °C· min^{-1}.

In situ CO adsorption FTIR was performed in a diffusion reflectance mode on a Nicolet iS10 FT-IR spectrometer with a mercury cadmium telluride (MCT) detector (spectral resolution of 4 cm^{-1} and accumulation of 32 scans). Prior to CO adsorption, about 10 mg sample was *in situ* reduced in a H_2 stream (30 ml min^{-1}) at 300 °C for 2 h and then purged by a N_2 stream (40 ml min^{-1}) at 300 °C for 1 h. After cooling to room temperature, CO adsorption was carried out in a flow of 10 vol.% CO/N_2 stream (40 ml min^{-1}) for 30 min, followed by purging with N_2 stream (40 ml min^{-1}) for 30 min. The IR spectra were collected.

Catalytic reaction test

Oxidation of toluene was conducted in a continuous down-flow fixed-bed micro-reactor under atmospheric pressure. Briefly, 100 mg catalyst (pressed and sieved 40–60 mesh) was pretreated in a H_2 stream (40 ml min^{-1}) at 300 °C for 2 h, then cooling to the 100 °C. Subsequently, toluene was metered by a microprocessor-controlled

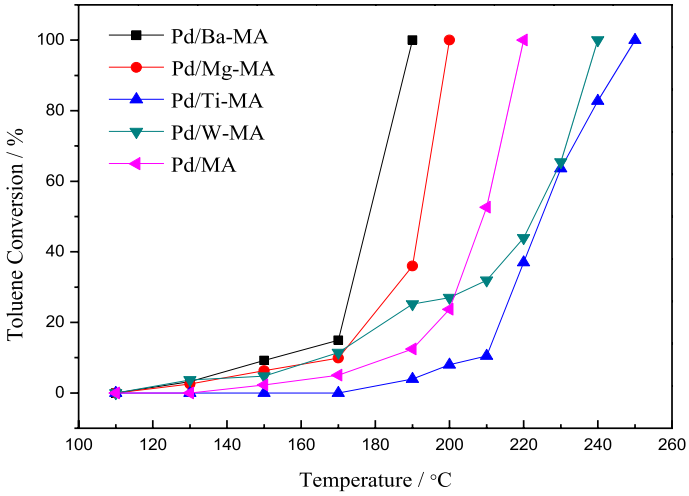

Fig. 1 The catalytic toluene oxidation performance of different samples

Table 1 Characteristic temperature of toluene oxidation with different samples

Catalysts	Characteristic temperature (°C)		
	T_{10}	T_{50}	T_{90}
Pd/Ba-MA	153	178	187
Pd/Mg-MA	168	192	198
Pd/Ti-MA	210	225	245
Pd/W-MA	170	223	237
Pd/MA	183	209	218

infusion pump and injected into a mixed flow gas at a rate of 0.0104 ml h^{-1}. The feed gas contains toluene 1000 ppm, 30% oxygen, 70% nitrogen, with a total flow of 40 ml min^{-1}, for a space velocity of 24,000 ml $g_{cat}{}^{-1}$ h^{-1}. The products were analyzed online by a gas chromatograph equipped with a Porapak Q packed column and a thermal conductivity detector (TCD). To get an accurate result, the reaction products were analyzed after 30 min reaction time on stream at least 3 times and the average value was used as the activity at each temperature.

Results and discussion

Catalytic reaction of toluene oxidation

Figure 1 shows the results of catalytic oxidation of toluene on Pd/MA catalyst doping with various acidic (Ti, W) and basic (Ba, Mg) elements. The toluene conversion temperatures T_{10}, T_{50} and T_{90} (T_{10}: temperature for 10% conversion, T_{50}:

temperature for 50% conversion and T_{90}: temperature for 90% conversion) of different catalysts are listed in Table 1. It can be seen from Fig. 1 and Table 1 that the catalytic activities of basic elements (Ba, Mg)-doped catalysts for toluene oxidation were higher than those of acid elements (Ti, W)-doped catalysts. Among them, Ba-doped Pd/Ba-MA catalyst had the highest activity, and the temperature of complete toluene conversion was 187 °C, while acid elements-doped catalysts had higher temperature (Pd/W-MA, T_{90} = 237 °C and Pd/Ti-MA, T_{90} = 245 °C, respectively) for the complete conversion than that of Pd/MA catalyst (T_{90} = 218 °C). The reason of the increase in catalytic activity of the catalyst doped with basic elements will be discussed in the later section.

BET and TEM analysis

Table 2 shows the specific surface areas, pore volumes and pore sizes of various supports. It shows that the specific surface area of catalyst increased by doping metal elements. Ti-MA had the largest specific surface area of 220 m^2/g among all catalysts. However, the catalytic activity of Ti-doped catalyst was much lower than that of Ba-doped catalyst, indicating that the activity of catalyst was not related to the specific surface area. As can be seen in the table, the pore volume and pore size of MA decreased by doping acidic and basic elements. The Ba-MA had the smallest pore volume of 0.38 m^2/g and pore size of 6.1 nm among all samples.

Figure 2 shows the TEM images of MA doped with different elements. It can be seen from Fig. 2a and c that basic elements Ba and Mg were uniformly dispersed on the mesoporous alumina, and the mesoporous structure of the support was not damaged. Figure 2b illustrates that the doping of W leaded to the collapse of the mesoporous structure of MA. Figure 2d shows that Ti element was evenly dispersed in MA, but the mesoporous structure of MA was collapsed. Figure 3 shows Pd particles were more dispersed on MA after the introduction of the additive. The introduction of Ba made Pd particles more disperse.

XRD analysis

Figure 4 shows the XRD patterns of the various samples. It can be seen from the figure that all the samples have the characteristic diffraction peaks of γ-Al_2O_3, among which the characteristic diffraction peaks of Mg-doped catalyst shifted to

Table 2 The pore structure of different supports

Supports	Surface area m^2/g	Pore volume cm^3/g	Pore size nm
MA	162	0.58	9.8
Ti-MA	220	0.53	7.1
W-MA	167	0.49	8.5
Mg-MA	204	0.51	6.5
Ba-MA	171	0.38	6.1

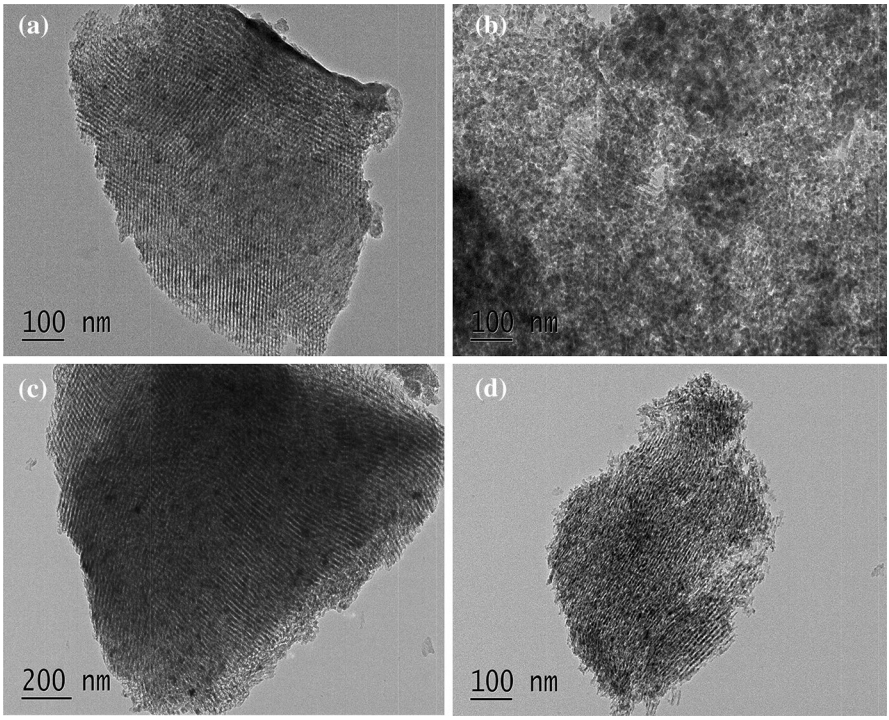

Fig. 2 TEM images of different supports, **a** Ba-MA, **b** W-MA, **c** Mg-MA, **d** Ti-MA

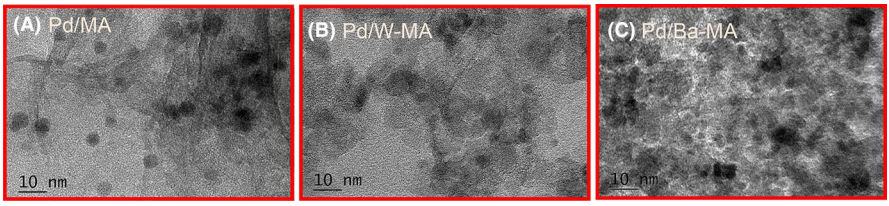

Fig. 3 TEM images of different catalyst, **a**. Pd-MA, **b**. Pd/W-MA, **c**. Pd/Ba-MA

the lower angle. This is because the ion radius of Mg^{2+} (72 pm) is larger than that of Al^{3+} (53.5 pm), the lattice of Al_2O_3 was expanded [33], and the diffraction peak moved to small diffraction angle. Moreover, based on the radius of Ba^{2+} (135 pm), Mg^{2+} (72 pm), Ti^{4+}(60 pm), W^{6+}(60.5 pm), Al^{3+} (53.5 pm), Ba^{2+} is difficult to insert into the crystal of γ-Al_2O_3 to form a complex, while Mg^{2+}, Ti^{4+} and W^{6+} are possible to insert into the crystal of γ-Al_2O_3 during the synthesis of M-MA. From the XRD patterns, new diffraction peaks at $2\theta = 18°$ and 28° were observed in Pd/Ba-MA sample, which is corresponding to the $BaAl_2O_4$ species, and it was in accordance with the previous report [34]. For other samples, Mg-MA, Ti-MA, W-MA show similar results with MA except a slight shift of

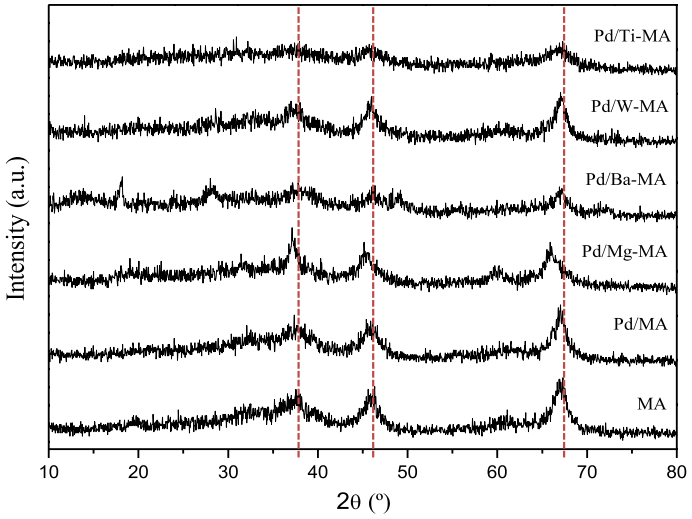

Fig. 4 XRD patterns of different catalysts

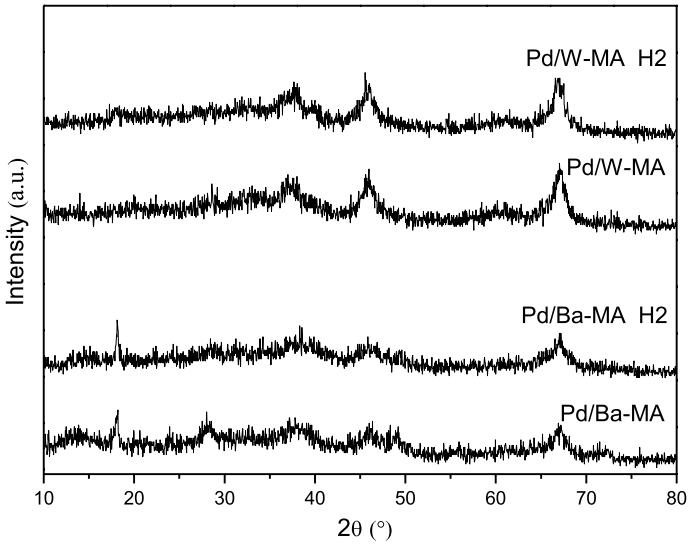

Fig. 5 XRD patterns of different catalysts before and after H_2 reduction

Mg-MA. It is related to their radius. The radius of Ti^{4+} and W^{6+} is close to the Al^{3+}, and the lattice parameter of γ-Al_2O_3 is basically invariable. On the contrary, the radius of Mg^{2+} is larger than that of Al^{3+}, and thus, the Mg-MA had the largest diffraction angle deviation.

Figure 5 shows the XRD of Pd/W-MA and Pd/Ba-MA before and after H_2 reduction. It can be seen from this figure that the characteristic peaks of γ-Al_2O_3 and the peaks of $BaAl_2O_4$ in Pd/Ba-MA had no change before and after H_2 reduction,

which suggests that the crystalline structure of the samples was stable during the H_2 reduction.

XPS analysis

The XPS spectra of Pd/Ba-MA, Pd/W-MA and Pd/MA are shown in Fig. 6. One can see that Pd $3d_{5/2}$ and Pd $3d_{3/2}$ of Pd/W-MA and Pd/MA are all near 336.7 eV and 342.0 eV, respectively, which belong to Pd^{2+}, indicating that PdO was the main species in both Pd/MA and Pd/M-MA samples. However, the binding energy of Pd in Pd/Ba-MA shifted to high energy, which is due to the formation of higher valence Pd species [5, 32–34]. The interaction between Pd and support was stronger in Pd/Ba-MA, resulting in the electron deficiency of Pd. This is consistent with our previous study [35].

In situ infrared analysis of CO adsorption

In order to investigate the electronic state of Pd species on the surface of catalyst doped with various elements, in situ infrared characterization of CO adsorption was carried out, and the results are shown in Fig. 7. The vibration peaks at 1978 cm^{-1} and 1950–1850 cm^{-1} were found in all catalysts, which were attributed to the bidentate bridge absorption peaks and tridentate bridge absorption peaks of CO. According to the literature [36], the bidentate bridge adsorption corresponds to the small Pd particles, while the tridentate bridge adsorption corresponds to the aggregated Pd particles. It can be seen from this figure that the intensity of tridentate bridge absorption peak of CO doped with acid elements Ti

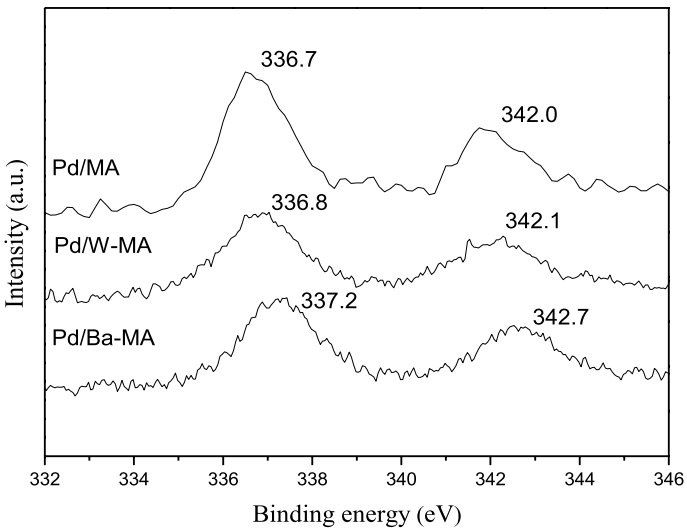

Fig. 6 Pd 3d XPS spectra of different catalysts

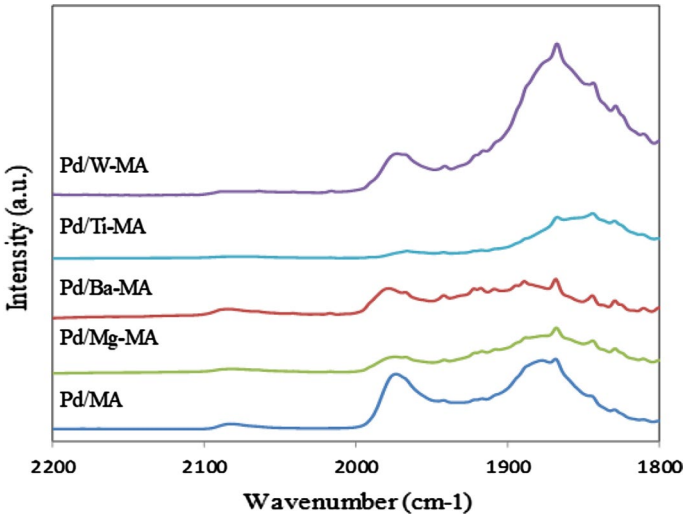

Fig. 7 IR spectra of in situ CO adsorption on different catalysts

and W was significantly higher than those of bidentate bridge absorption peak, indicating that there were more aggregated Pd particles on the surface of catalyst. However, the tridentate bridge absorption peak of the catalyst doped with basic element was very weak, which indicated that Pd mainly existed in the form of small particles. The results show that the doping of acidic elements resulted in the aggregation of Pd particles, while the doping of alkaline elements promoted the dispersion of Pd particles. Xie et al. [37] reported the similar results.

H_2-TPR analysis

The chemical state of Pd could affect the catalytic activity of Pd-based catalysts. Some reports suggested that Pd^0 is the active site of catalytic oxidation [38–40], while others suggested that oxide state (PdO/Pd^{2+}) is the active site. [41, 42] It is usually difficult to distinguish the valence state of Pd, because Pd is prone to oxidation/reduction conversion ($Pd \leftrightarrow PdO$) in the process of high temperature catalytic oxidation [43, 44]. In order to study the influence of acid–base doping elements on the catalytic oxidation activity of toluene, we characterized all the catalysts by H_2-TPR. The results are shown in Fig. 8. In general, PdO can be reduced to metal Pd at a temperature below 200 °C [45, 46]. Thus, the reduction peak below 80 °C in the TPR profile belongs to the reduction of PdO species. It shows that the reduction temperatures of Ba- and Mg-doped catalysts were similar to that of Pd/MA, ~ 65 °C, while the reduction temperatures of Ti- and W-doped catalysts were ~ 71 °C. In addition, the peak areas of the catalysts doped with basic elements were greater than those doped with acidic elements. The results suggested that the reducible PdO increased in the basic elements-doped catalysts.

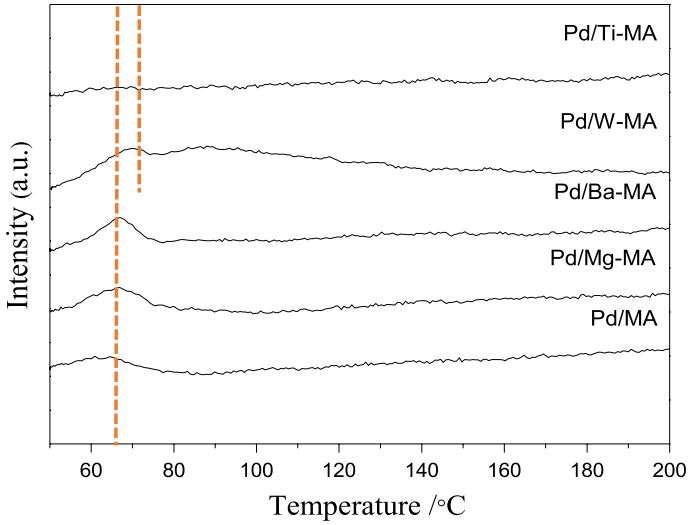

Fig. 8 H_2 -TPR profiles of different catalysts

Conclusion

In this work, MA support was doped with acidic (Ti, W) or alkaline (Ba, Mg) elements. The Pd catalysts were prepared by incipient-wetness impregnation method. The influence of the doped elements on the Pd catalysts for the toluene oxidation was investigated through BET, TEM, XRD, XPS, in situ CO-IR and H_2-TPR. For the toluene oxidation, the catalysts doped with basic elements had lower starting combustion temperature and complete conversion temperature than those of catalysts doped with acidic elements, among which the Pd/Ba-MA catalyst had the lowest complete conversion temperature of 187 °C. The results of in situ CO adsorption FTIR indicated that the doping of basic elements was beneficial to the dispersion of PdO particles, while the doping of acidic elements suppressed the dispersion of PdO particles. In addition, the binding energy of Pd in Pd/Ba-MA shifted to high energy, indicating that the interaction between PdO and Ba-MO support was enhanced. The results of H_2-TPR showed that the reducibility of catalysts doped with alkaline elements was stronger than those doped with acidic elements. In conclusion, the MO support doped with basic elements promoted the dispersion of PdO particles, changed the electronic state of Pd and enhanced the reducibility of PdO, which ultimately led to its high activity.

Acknowledgements This work was supported by the National Key Research and Development Program of China (2016YFC0204301), the National Natural Science Foundation of China (21976082, 21607122) and the Key Research and Development Program of Jiangsu Province of China (BE2019118).

References

1. M.S. Kamal, S.A. Razzak, M.M. Hossain, Atmos. Environ. **140**, 117 (2016)
2. C. Yang, G. Miao, Y. Pi, Q. Xia, J. Wu, Z. Li, Chem. Eng. J. **370**, 1128 (2019)
3. A.C. Lewis, N. Carslaw, P.J. Marriott, R.M. Kinghorn, P. Morrison, Nature **405**, 778 (2000)
4. X. Zhang, B. Gao, A.E. Creamer, C. Cao, Y. Li, J. Hazard. Mater. **338**, 102 (2017)
5. P. Li, C. He, J. Cheng, C.Y. Ma, B.J. Dou, Z.P. Hao, Appl. Catal. B Environ. **101**, 570 (2011)
6. L.F. Liotta, Appl. Catal. B Environ. **100**, 403 (2010)
7. S. Scire, L.F. Liotta, Appl. Catal. B Environ. **125**, 222 (2012)
8. C. Song, M. Chen, C. Ma, X. Zheng, Chin. J. Chem. **27**, 1903 (2009)
9. S. Mohammad, I. Mohammad, Chin. J. Chem. **28**, 2216 (2010)
10. Y. Xia, H. Dai, H. Jiang, L. Zhang, Catal. Commun. **11**, 1171 (2010)
11. W. Si, Y. Wang, Y. Peng, X. Li, K. Li, J. Li, Chem. Commun. **51**, 14977 (2015)
12. S.C. Kim, C.Y. Park, Res. Chem. Intermed. **28**, 441 (2002)
13. Y.T. Lai, T.C. Chen, Y.K. Lan, B.S. Chen, J.H. You, C.M. Yang, N.C. Lai, J.H. Wu, C.S. Chen, ACS Catal. **4**, 3824 (2014)
14. H. Huang, X. Ying, Q. Feng, D.Y.C. Leung, Catal. Sci. Technol. **5**, 2649 (2015)
15. C. Zhu, L. Jing, Y. Peng, L. Jingrong, Chem. Eng. J. **356**, 255 (2019)
16. Z. Wu, J. Deng, S. Xie, H. Yang, X. Zhao, K. Zhang, H. Lin, H. Dai, G. Guo, Microporous Mesoporous Mater. **224**, 311 (2016)
17. H. Huang, D.Y.C. Leung, ACS Catal. **1**, 348 (2011)
18. M.Y. Byun, J.S. Kim, D.W. Park, M.S. Lee, J. Nanosci. Nanotechnol. **18**, 6283 (2018)
19. Z. Zhen, R.J. Wu, J. Taiwan Inst. Chem. E. **50**, 276 (2015)
20. M.C. Álvarez-Galván, B. Pawelec, V.A.D. O'Shea, J.L.G. Fierroa, P.L. Arias, Appl. Catal. B Environ. **51**, 83 (2004)
21. W. Cho, Y. Nbaek, Y.C. Kim, M. Zuanpo, Res. Chem. Intermed. **28**, 343 (2002)
22. T. Barakat, J.C. Rooke, R. Cousin, J.F. Lamonier, J.M. Giraudon, B.L. Su, S. Sinert, New J. Chem. **38**, 2066 (2014)
23. R. Pellegrini, G. Leofanti, G. Agostini, E. Groppo, M. Rivallan, C. Lamberti, Langmuir **25**, 6476 (2009)
24. L. Ilieva, J.W. Sobczak, M. Manzoli, B.L. Su, D. Andreeva, Appl. Catal. A Gen. **291**, 85 (2005)
25. J. Cejka, Appl. Catal. A Gen. **254**, 327 (2003)
26. C. Márquez-Alvarez, N. Žilková, J. Pérez-Pariente, J. Čejka, Catal. Rev. **50**, 222 (2008)
27. C.K. Sang, G.S. Wang, Appl. Catal. B Environ. **92**, 429 (2009)
28. K. Okumura, T. Kobayashi, H. Tanaka, M. Niwa, Appl. Catal. B: Environ. **44**, 325 (2003)
29. R.G. Derwent, M.E. Jenkin, S.M. Saunders, Atmos. Environ. **32**, 2429 (1998)
30. Y. Wang, C. Zhang, F. Liu, H. Hong, Appl. Catal. B Environ. **142**, 72 (2013)
31. G.H. Kim, K.D. Jung, W. Kim, B.H. Um, Res. Chem. Intermed. **42**(1), 351 (2015)
32. C. Zhang, Y. Li, Y. Wang, H. He, Environ. Sci. Technol. **48**, 5816 (2014)
33. S. He, Y. Cui, Y. Yao, R. Fang, Z. Shi, M. Gong, Y.Q. Chen, Acta Phys. Chim. Sin. **27**, 1157 (2011)
34. Y. Cao, R. Rui, X. Wu, W. Duan, Appl. Catal. A Gen. **501**, 17 (2015)
35. X. Weng, B. Shi, A. Liu, J. Sun, Y. Xiong, H. Wan, S. Zheng, L. Dong, Y. Chen, Appl. Surf. Sci. **497**, 143747 (2019)
36. J. Sun, Y. Han, H. Fu, X. Qu, Z. Xu, S. Zheng, Chem. Eng. J. **313**, 1 (2017)
37. J. Xie, J. Wang, W. Hui, L. Hang, J. Wang, M. Shen, Catal. Lett. **148**, 2596 (2018)
38. S. Huang, C. Zhang, H. Hong, Catal. Today **139**, 15 (2008)
39. S.K. Ihm, Y.D. Jun, D.C. Kim, K.E. Jeong, Catal. Today **93**, 149 (2004)
40. G.S. Wang, J.W. Lee, C.K. Sang, Appl. Catal. B Environ. **84**, 133 (2008)
41. S.C. Su, J.N. Carstens, A.T. Bell, J. Catal. **176**, 125 (1998)
42. R.J. Farrauto, J.K. Lampert, M.C. Hobson, E.M. Waterman, Appl. Catal. B Environ. **6**, 263 (1995)
43. P.O. Thevenin, A. Alcalde, L.J. Pettersson, S.G. Järås, J.L.G. Fierro, J. Catal. **215**, 78 (2003)
44. Z. Zhang, M. Chen, W. Shangguan, Catal. Commun. **10**, 1330 (2009)
45. S. Komhom, O. Mekasuwandumrong, P. Praserthdam, J. Panpranot, Catal. Commun. **10**, 86 (2008)
46. J. Pu, F. Liang, B. Hua, Y. Dong, B. Chi, J. Li, Rare Metal Mater. Eng. **39**, 1396 (2010)

Affiliations

Chengyan Ge[1,2] · Lixia Xu[2] · Jingfang Sun[2] · Hongxia Liu[1] · Qing Tong[2] · Weixin Zou[2] · Changjin Tang[2] · Haiqin Wan[2] · Lin Dong[2] · Yu-Wen Chen[3]

[1] School of Chemistry and Chemical Engineering, Yancheng Institute of Technology, Yancheng 224000, People's Republic of China

[2] School of the Environment, Jiangsu Key Laboratory of Vehicle Emissions Control, Center of Modern Analysis, School of Chemistry and Chemical Engineering, Nanjing University, Nanjing 210093, People's Republic of China

[3] Department of Chemical and Materials Engineering, National Central University, Jhong-Li 32001, Taiwan, ROC